Available online at www.sciencedirect.com
SCIENCE DIRECT®
Journal of Nuclear Materials 345 (2005) 46–64
journal of nuclear materials
www.elsevier.com/locate/jnucmat

Leach testing at 50 °C of α-doped SON68 glass alteration gels

Patrick Jollivet *, Géraldine Parisot

CEA Marcoule, Laboratoire de Comportement à Long Terme, BP 17171, 30207 Bagnols-sur-Cèze cedex, France

Received 26 January 2005; accepted 4 May 2005

Abstract

Gels formed by altering α-doped (Np, Pu, Am) SON68 glass at 300 °C were leached during 1 year at 44 cm^{-1} and 50 °C under oxidizing conditions ($Eh_{/NHE} \approx +150$ mV) and under reducing conditions ($Eh_{/NHE} \approx -250$ mV). After 3 days of leaching the gel dissolution was highly incongruent. The gel dissolution rate calculated from the silicon concentrations was 4.4×10^{-5} g m^{-2} d^{-1}, except for the Am-doped gel, for which the rate was two times higher. During leaching, Np is weakly retained in the gel (35% under oxidizing conditions and 50% under reducing conditions) whereas Pu and Am are strongly retained (over 90%). The three lanthanides La, Ce, and Nd exhibit exactly the same leaching behavior, but different from that of actinides. Speciation and complexation calculations for neodymium showed that its solubility could be controlled by $Nd(OH)_3$ for periods beyond 3 months. Conversely, no simple chemical compound appears to control the solubility of the actinides.

1. Introduction

Radionuclides are retained in various degrees in the gels that form during SON68 glass alteration. In the case of the rare earth elements and actinides, retention in the gels can significantly diminish the glass source term. The radioelement containment stability in the gels must be assessed in order to take radionuclide retention into account in glass package performance calculations. Radionuclide retention depends on the conditions in which the gels are formed. The main objectives of this study were to assess the influence of the oxidation–reduction potential Eh of the solution on the release of the multivalent actinides Np and Pu, to determine the influence of α and βγ self-irradiation in the gel pores on the gel dissolution rate and to check if the long term actinides concentrations in solution were controlled by simple phases. The gels were obtained by complete alteration at 300 °C of SON68 glass specimens doped with NpO_2, PuO_2 and Am_2O_3. The three gels were then leached at 50 °C under oxidizing conditions to determine their stability under self-irradiation. The Np- and Pu-doped gels were also leached under reducing conditions to investigate actinide release versus the oxidation–reduction potential in solution.

2. Gel fabrication and characterization

Four gels were obtained by altering glass under static hydrothermal conditions in stainless steel reactors with gold seals. An inactive SON68 glass coupon and three SON68 glass coupons doped with α-emitters (^{237}Np,

* Corresponding author. Tel.: +33 4 66 79 63 73; fax: +33 4 66 79 66 20.
E-mail address: patrick.jollivet@cea.fr (P. Jollivet).

0022-3115/$ - see front matter © 2005 Elsevier B.V. All rights reserved.
doi:10.1016/j.jnucmat.2005.05.011

^{239}Pu and ^{241}Am) were altered at 300 °C under 100 bars. Three glass monoliths ($25 \times 25 \times 3$ mm^3) representing a surface area of 45 cm^2 were placed in each reactor in a solution volume of 40 cm^3 to obtain an SA/V ratio of 1.1 cm^{-1}. The glass monoliths were completely altered within 72 days. After alteration, the glass monoliths had doubled in volume and were extensively cracked. The gels were oven-dried for 1 day at 90 °C, then manually ground with a mortar and a pestle. The specific surface area of an inactive gel sample measured by krypton adsorption using the BET method was 4.4 m^2 g^{-1}. The specific surface areas of the α-doped gels were not measured; the value obtained for the inactive gel was used, as all four gels were ground in the same way.

SEM observation of the inactive gel revealed secondary phases consisting of needles and sheets mixed with the gel itself, as shown in Fig. 1. Afterwards, the word gel will refer to the amorphous material including the crystallized phases. The X-ray diffraction pattern (Fig. 2) shows that the Np-doped gel was mainly amorphous (bump between 10° and 40°) and contained crystallized phases. The X-ray diffraction patterns of inactive, Np-, Pu-, Am-doped gels were identical. The following phases were identified:

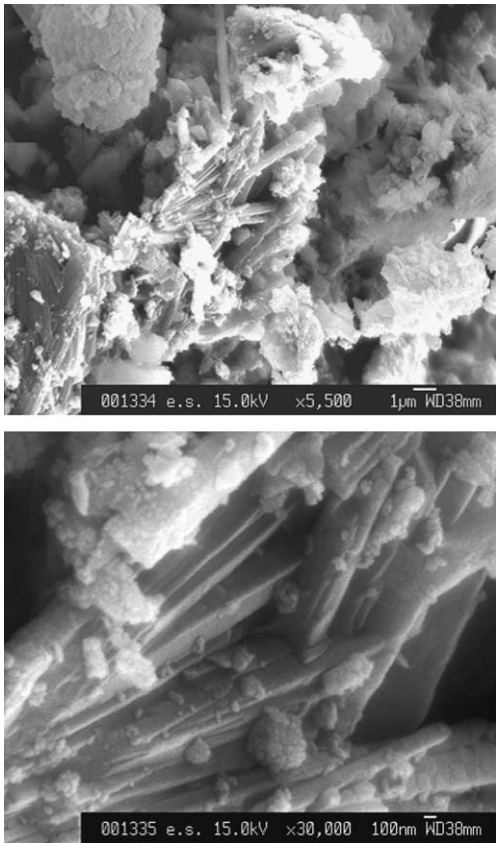

Fig. 1. SEM image of inactive gel.

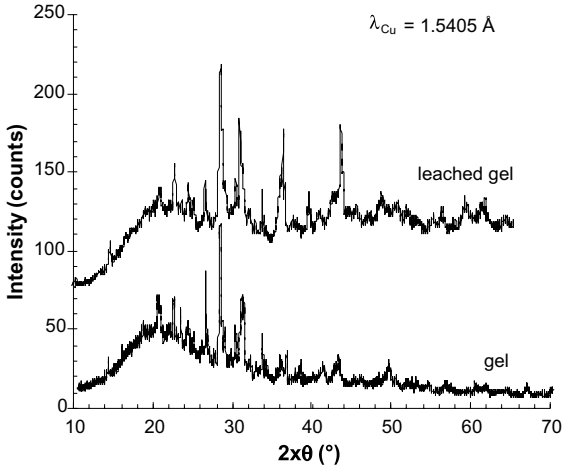

Fig. 2. X-ray diffraction pattern of Np-doped gel before and after leaching.

- analcime $Na_{14.80}Al_{14.24}Si_{33.76}O_{96}(H_2O)_{16}$,
- intermediate albite $NaAlSi_3O_8$,
- low calcian albite $Na_{0.84}Ca_{0.16}Al_{1.16}Si_{2.84}O_8$,
- labradorite $Ca_{0.64}Na_{0.35}Al_{1.63}Si_{2.37}O_8$,
- $Ca_{8.25}Na_{1.5}Al_6O_{18}$,
- acmite $NaFeSi_2O_6$.

The crystallized phases could not be quantified by XRD analysis for lack of calibration but SEM observations showed that these crystallized phases were very few (in quantity) compared to amorphous material. The diffraction pattern of the leached Np-doped gel (Fig. 2) includes additional peaks at 36.42°, 39.67° and 43.69° ($2 \times \theta$) not found in unleached gel, indicating the presence of rare earth phosphates after leaching.

The chemical composition of the inactive gel (amorphous material and crystallized phases) was very near that of SON68 glass (Table 1), with only a lower boron and sodium content in the gel than in the glass and the presence of an appreciable quantity of water (≈6 mol%) in the gel. The measured silicon retention in the gel was 81%. The chemical compositions of the α-doped gels could not be analyzed, but were assumed to have the same composition as the inactive gel, considering that all four gels were obtained under the same conditions with the exception of the actinide content. The actinide content of the α-doped gels was calculated from the material balance as the difference between the quantity of actinide in the glass and the quantity found in solution. The actinide weight percentages in the gel samples are indicated in Table 2.

In the same time, another gel was obtained by complete alteration of inactive SON68 glass powder (granulometric size ranged from 3 to 25 μm) in pseudo-dynamic mode (renewal rate of 0.25 d^{-1}) at 30 cm^{-1} and 90 °C during about 1 year. The silicon

Table 1
Mass and molar composition of inactive gel obtained at 300 °C (O calculated as remainder; Co, Ag, Cd, Sn, Sb ignored)

Element	wt%	mol%
Si	22.79	17.90
Al	2.47	2.02
B	1.62	3.30
Na	5.51	5.29
Ca	3.40	1.87
Li	0.88	2.79
Zn	2.60	0.88
Zr	2.62	0.63
Fe	2.58	1.02
Ni	0.76	0.29
Cr	0.39	0.17
P	0.26	0.19
U	0.23	0.02
Th	0.36	0.03
Sr	0.36	0.09
Y	0.21	0.05
Mo	0.31	0.07
Mn	0.58	0.23
Te	0.17	0.03
Cs	1.77	0.29
Ba	0.60	0.10
La	0.97	0.15
Ce	1.04	0.16
Pr	0.51	0.08
Nd	1.44	0.22
H_2O	4.86	5.95
O	40.71	56.15

Table 2
Actinide concentrations (wt%) in the gels

Material	U + Th	^{237}Np	$^{239+240}Pu$	^{241}Am
nr-gel[a]	0.59	–	–	–
Np-gel	–	0.85	–	–
Pu-gel	–	–	0.74 (0.57 + 0.17)	–
Am-gel	–	–	–	0.79

[a] nr-gel: Non-radioactive gel.

retention in this gel was about 22%; this value is much lower than that of gels formed at 300 °C because of the large flow rate used to transform glass into gel at 90 °C. More, the gel formed at 90 °C does not contain the crystallized phases formed at 300 °C; just the presence of thin sheets of phyllosilicates at the surface of the amorphous gel grains is observed.

3. Gel leaching

The gels were leached during 1 year at 50 °C in ultrapure water (18 MΩ cm) in static mode without stirring. All four gel samples were leached under oxidizing conditions in PTFE reactors. The leaching solution volume was 1000 cm^3 for 1.00 g of gel. The Np- and Pu-doped gels were also leached under reducing conditions in stainless steel reactors with viton seals, with a leaching solution volume of 500 cm^3 for 0.50 g of gel. All the leach tests were therefore carried out with an initial SA/V ratio of 44 cm^{-1}. All the experiments were carried out in a glove box under air and the atmosphere inside the reactors was air for oxidizing medium and hydrogenated argon for reducing medium. Reducing conditions were obtained by periodically purging the reactors with argon containing 7% hydrogen (Fig. 3). After each solution analysis sample was taken, the reactors were purged with hydrogenated argon for about 3 h at a rate of 20 L h^{-1}.

Several solution samples were taken at each interval for analysis as follows:

- 3 cm^3 of unfiltered solution for pH and Eh measurement,
- 5 cm^3 of unfiltered solution for ICP-AES and α spectrometry,
- 2 cm^3 of solution filtered to 0.45 μm for α spectrometry,
- 5 cm^3 of solution ultrafiltered to 10 000 Daltons for ICP-MS, ICP-AES (Si, Na, Ca, Al) and α spectrometry.

All the samples for ICP-AES, ICP-MS and α spectrometry analyses were acidified with HNO_3 at a pH value of 1, just after sampling.

At the end of the experiments under reducing conditions, the two stainless steel reactors were rinsed with HNO_3 1 N. The activity fixed on the walls of the reactors (roughness less than 1 μm) for Np and Pu was respectively less than 5% and 20% of the activity measured in the ultrafiltered samples after 1 year of leaching.

As for inactive gels formed at 90 °C, they were also leached at 50 °C in ultrapure water during 2 years at SA/V ratios of 130 and 2500 cm^{-1}, in static mode without stirring and under oxidizing conditions. The goal of these leachings was to compare the dissolution rates of gels formed at 300 °C (including crystallized phases) to

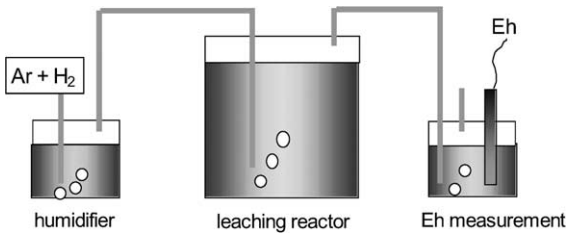

Fig. 3. Gel leaching setup under reducing conditions.

those of gel formed at 90 °C (without these crystallized phases).

4. Results

4.1. pH

The pH values measured at 50 °C in unfiltered solution samples (Fig. 4) are indicated within ±0.1 unit. The pH variation measured over time during leaching under oxidizing conditions shows a slight decrease in the pH (about 0.3 unit) between 1 day and 6 months, after which the pH remained constant to 1 year. The same pattern was observed for the four gels. The pH observed during the leaching of the inactive, Np- and Pu-doped gels was about 8.8 ± 0.1 whereas the value measured for Am-doped gel was about 0.5 unit lower. This phenomenon was due to gamma radiolysis of the N_2–O_2–H_2O system leading to the formation of nitric acid among other compounds [1,2] and to γ radiation-induced effects on carbonate–bicarbonate–CO_2(g) equilibrium [3]. Under reducing conditions, the overall pH variation during leaching of Pu-doped gel was similar to the trend observed during the test under oxidizing conditions, except that the values measured between 3 months and 1 year were lower by about 0.3 unit on average. Conversely, the pH for the Np-doped gel increased from 6 to slightly over 9 between 1 day and 1 month, then remained roughly constant at about 0.5 unit above the values obtained under oxidizing conditions.

The leaching solution pH variation over time was simulated using the pH calculation module of the LIXIVER code [4] to estimate the CO_2 fugacity at equilibrium with the leachate. In these calculations, the input data were the measured elements concentrations and the CO_2 fugacity was fitted by successive iterations until the calculated pH equalled the measured one. The following equilibria have been taken into account for the CO_2 fugacity calculation:

$$CO_2(g) + H_2O \leftrightarrows HCO_3^- + H^+ \quad \beta_1^{50^\circ} = 10^{-8.01} \quad [5]$$

$$CO_3^{2-} + H^+ \leftrightarrows HCO_3^- \quad \beta_2^{50^\circ} = 10^{16.16} \quad [5]$$

For the gels leached under oxidizing conditions, the CO_2 fugacity at equilibrium with the leachate increased over time to reach the atmospheric P_{CO_2} value, as shown in Fig. 5 for the inactive gel. During gel leaching under oxidizing conditions, the carbonates were initially consumed very rapidly by gel dissolution elements and as the PTFE reactors were not airtight, the leachate eventually reached equilibrium with the atmosphere. For the Am-doped gel, a carbon dioxide fugacity equal to the atmospheric P_{CO_2} was not sufficient to obtain the pH measured experimentally. This confirms the effect of gamma radiolysis due to americium.

The CO_2 fugacity calculated during leaching of Pu-doped gel under reducing conditions (Fig. 5) varied in the same way as the values calculated for oxidizing conditions. Conversely, for the Np-doped gel, the CO_2 fugacity (Fig. 5) diminished over time. Considering the operating procedure (hydrogenated argon purging) and the reactors used for leaching under reducing conditions, the fugacity variation for the Np-doped gel appears more logical than the result obtained for Pu-doped gel. It is reasonable to expect a drop in the carbon dioxide fugacity in the leachate. The difference between Np- and Pu-doped gels could be attributable to a pH measurement error in the plutonium-doped gel leachate,

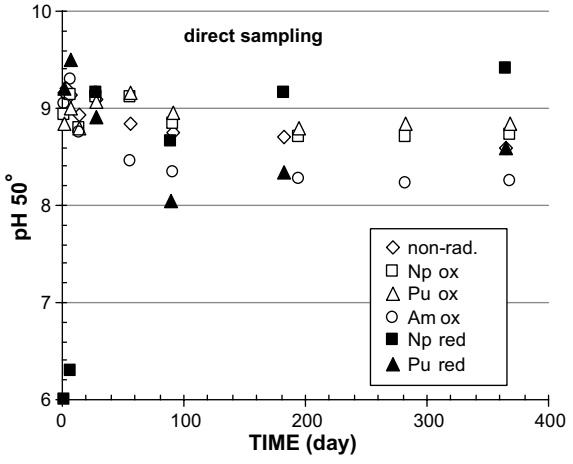

Fig. 4. pH versus time at 50 °C during gels leaching under oxidizing and reducing conditions.

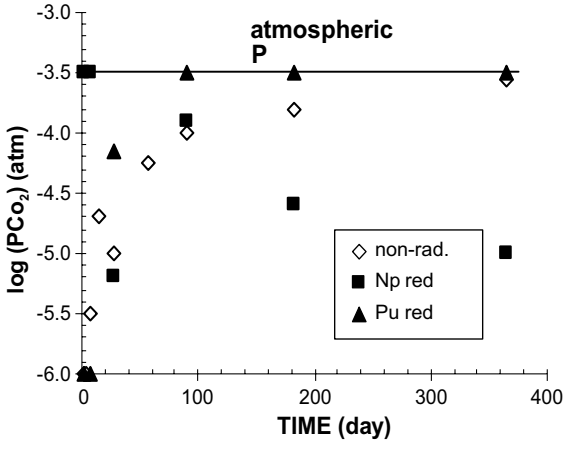

Fig. 5. Logarithm of CO_2 partial pressure versus time, calculated at equilibrium with leachates for inactive gel (non-rad.) under oxidizing conditions and for Np- and Pu-doped gels under reducing conditions.

or, more probably, to a carbon dioxide intake in the leaching reactor during the hydrogenated argon bubbling.

4.2. Eh

The oxidation–reduction potentials were measured at 50 °C with respect to the standard hydrogen electrode. The Eh values were constant during whole the duration of leaching, as well for oxidizing as for reducing conditions. The Eh values in the leachate under oxidizing conditions were about +150 mV regardless of the leaching time and irrespective of the actinide. Under reducing conditions, the oxidation–reduction potential values were measured in the Eh measurement vessel (Fig. 3) after the hydrogenated argon bubbling. The leachate $Eh_{/NHE}$ values were −230 mV for the Np-doped gel and −280 mV for the Pu-doped gel. Just after each sampling, the Eh value was also measured in the 3 cm^3 sample. This measurement took about 2–3 min and the Eh value was still negative (although the glove box was under air and not inert gas), indicating that the solution in the leaching reactors was really reducing.

4.3. Element concentrations

The unfiltered concentrations exceeded the ultrafiltered concentrations, except for B, Na and Li. The unfiltered concentrations of the sparingly soluble elements (Al, Fe, Zr, La, Ce, Nd) decreased from 0 to 28 days, then remained roughly constant. This phenomenon can be attributed to the presence of fine gel particles in suspension in the initial leachate samples. The gels were not screened to eliminate the smallest particles before they were placed in the reactors.

The variation over time of the ultrafiltered concentrations (Tables 3–8) allows the elements to be classified into two broad categories based on their leaching behavior. The first comprises elements with concentrations that increased continuously over time up to 1 year, and includes Si, Na, Li, Cs, Ca, and Sr. The second comprises elements with concentrations that increased very slightly over time, such as Zr, La, Ce, Nd, Al, and Fe. Boron exhibited a different behavior: all the boron present in the gels was released into solution from day 1, after which the concentrations (unfiltered or ultrafiltered) remained constant over time. The boron release into solution was thus related neither to the dissolution of the gels nor to the crystallized phases formed during glass alteration. The solubility of aluminum was about 0.3 ppm, compared with nearly 1 ppm for iron. The same values are observed during SON68 glass alteration [6]. Taking into account the composition of the leachate, the aluminium and iron solubilities were calculated using the geochemical CHESS code [7]. These calculations led to Al and Fe concentrations in solution more

Table 3
Ultrafiltered concentrations versus time during leaching of inactive gel under oxidizing conditions

Time (Day)	Si ($mg\,L^{-1}$)	B ($mg\,L^{-1}$)	Na ($mg\,L^{-1}$)	Li ($mg\,L^{-1}$)	Ca ($mg\,L^{-1}$)	Sr ($mg\,L^{-1}$)	Al ($mg\,L^{-1}$)	Fe ($mg\,L^{-1}$)	Zr ($mg\,L^{-1}$)	La ($mg\,L^{-1}$)	Ce ($mg\,L^{-1}$)	Nd ($mg\,L^{-1}$)	Cs ($mg\,L^{-1}$)
1	7.6	9.8	8.7	0.74	0.52	0.05	0.34	1.1	–	–	–	–	–
3	5.1	9.7	8.3	0.55	0.57	0.03	0.10	0.26	–	–	–	–	–
7	8.5	10.1	9.8	0.82	1.8	0.09	0.35	0.84	0.4	0.8	0.8	1.4	5.7
14	6.5	10.2	9.9	0.70	1.9	0.09	0.48	0.01	–	–	–	–	–
28	7.9	10.2	10.2	0.82	2.6	0.82	0.03	<0.01	–	–	–	–	–
57	10.0	10.2	10.6	1.1	3.7	0.12	0.02	<0.01	–	–	–	–	–
91	12.6	10.2	11.2	1.5	4.8	0.10	<0.01	<0.01	0.04	<0.01	<0.01	0.01	2.5
183	15.6	10.3	12.1	2.2	6.9	0.20	0.04	<0.01	0.01	<0.01	<0.01	0.01	2.6
365	18.0	10.2	13.2	3.3	9.4	<0.01	<0.1	<0.01	<0.01	<0.01	<0.01	<0.01	<0.01

Table 4
Ultrafiltered concentrations versus time during leaching of Np-doped gel under oxidizing conditions

Time (Day)	Si (mg L^{-1})	B (mg L^{-1})	Na (mg L^{-1})	Li (mg L^{-1})	Ca (mg L^{-1})	Sr (mg L^{-1})	Al (mg L^{-1})	Fe (mg L^{-1})	Zr (μg L^{-1})	La (μg L^{-1})	Ce (μg L^{-1})	Nd (μg L^{-1})	Cs (mg L^{-1})
1	8.6	12.9	17.8	0.74	1.48	<0.2	0.49	0.40	23.5	4.9	6.6	9.0	1.38
7	8.0	10.2	12.5	0.84	0.76	<0.2	0.30	0.70	10.3	2.5	3.3	4.0	1.90
14	10.7	9.8	17.6	1.04	0.67	<0.2	0.22	0.48	9.2	8.8	10.0	17.0	2.62
28	7.3	13.2	18.1	1.27	1.46	<0.2	0.24	0.35	8.2	2.5	2.9	3.8	3.08
56	16.8	9.8	19.7	1.53	3.89	<0.2	0.85	0.75	10.9	26.7	29.3	53.2	3.32
92	14.3	9.6	16.1	1.62	3.70	<0.2	0.23	0.35	12.4	2.5	3.7	5.1	3.38
194	16.7	9.4	13.3	2.16	5.28	<0.2	0.31	1.18	12.6	10.9	12.7	21.9	3.58
282	25.8	13.0	23.7	3.63	11.30	<0.2	0.41	0.85	10.7	4.0	5.1	7.8	5.52
369	21.3	9.6	16.5	2.98	9.50	<0.2	0.32	0.45	14.0	<2.5	<2.5	<2.5	4.04

Table 5
Ultrafiltered concentrations versus time during leaching of Pu-doped gel under oxidizing conditions

Time (Day)	Si (mg L^{-1})	B (mg L^{-1})	Na (mg L^{-1})	Li (mg L^{-1})	Ca (mg L^{-1})	Sr (mg L^{-1})	Al (mg L^{-1})	Fe (mg L^{-1})	Zr (μg L^{-1})	La (μg L^{-1})	Ce (μg L^{-1})	Nd (μg L^{-1})	Cs (mg L^{-1})
1	10.2	8.6	9.1	1.47	0.80	<0.2	0.29	0.68	12.6	3.0	4.0	5.3	<0.2
7	21.2	17.6	17.8	3.32	0.60	<0.2	0.19	1.02	12.6	3.6	4.8	6.5	<0.2
14	23.1	18.2	19.8	3.38	0.74	<0.2	0.24	1.19	19.3	3.5	5.4	6.4	<0.2
28	25.5	19.4	21.9	3.59	0.90	<0.2	0.30	0.84	11.7	2.5	3.0	3.8	<0.2
56	28.5	28.0	31.6	3.95	0.82	<0.2	0.32	1.29	7.8	2.5	2.5	3.3	<0.2
92	33.7	21.8	33.7	4.10	1.25	<0.2	0.38	0.33	17.2	7.0	8.5	14.3	0.2
194	34.1	29.6	39.7	5.84	3.30	<0.2	2.20	1.07	31.0	4.9	8.3	9.4	0.31
282	37.8	25.2	38.0	5.00	2.00	<0.2	0.31	0.80	17.5	3.0	3.5	6.4	0.29
369	37.2	24.6	34.4	5.11	1.85	<0.2	0.10	1.64	5.7	<2.5	<2.5	<2.5	0.31

Table 6
Ultrafiltered concentrations versus time during leaching of Am-doped gel under oxidizing conditions

Time (Day)	Si (mg L^{-1})	B (mg L^{-1})	Na (mg L^{-1})	Li (mg L^{-1})	Ca (mg L^{-1})	Sr (mg L^{-1})	Al (mg L^{-1})	Fe (mg L^{-1})	Zr (μg L^{-1})	La (μg L^{-1})	Ce (μg L^{-1})	Nd (μg L^{-1})	Cs (mg L^{-1})
1	17.5	6.58	13.9	1.19	0.60	<0.2	0.13	1.10	12.0	<2.5	<2.5	2.5	0.41
7	25.0	7.22	17.6	1.39	1.94	<0.2	0.47	0.70	14.5	<2.5	3.3	4.0	0.50
14	25.1	7.60	18.8	1.65	1.08	<0.2	0.22	<0.2	8.3	<2.5	2.5	4.5	0.67
28	24.8	7.60	16.6	1.77	1.39	<0.2	0.18	0.37	22.3	4.8	7.3	8.8	0.84
56	24.4	9.66	21.1	2.59	3.89	0.28	0.60	0.29	20.8	4.5	6.8	9.5	1.26
92	34.3	8.62	13.9	2.72	5.25	0.36	0.41	<0.2	16.0	<2.5	2.8	3.0	1.28
194	46.2	10.20	26.4	4.72	7.73	0.50	0.73	<0.2	20.5	4.0	5.5	9.8	1.56
282	–	13.28	–	7.14	–	0.63	–	0.25	23.3	3.5	4.8	6.5	2.06
369	–	17.60	–	10.02	–	0.91	–	–	26.5	7.3	7.8	14.0	2.64

Table 7
Ultrafiltered concentrations versus time during leaching of Np-doped gel under reducing conditions

Time (Day)	Si (mg L^{-1})	B (mg L^{-1})	Na (mg L^{-1})	Li (mg L^{-1})	Ca (mg L^{-1})	Sr (mg L^{-1})	Al (mg L^{-1})	Fe (mg L^{-1})	Zr (μg L^{-1})	La (μg L^{-1})	Ce (μg L^{-1})	Nd (μg L^{-1})	Cs (mg L^{-1})
1	–	14.6	–	0.91	–	<0.2	–	0.86	38.3	10.8	16.2	19.6	1.67
7	8.4	8.2	9.9	0.76	0.18	<0.2	<0.1	0.74	3.0	4.8	4.5	8.0	1.73
28	9.0	8.2	12.6	1.07	0.35	<0.2	0.13	0.46	20.1	2.7	6.1	4.8	2.50
90	15.6	10.2	16.0	1.75	1.58	<0.2	0.19	0.88	2.9	<2.5	<2.5	3.0	3.18
182	12.6	8.6	5.0	2.03	3.34	<0.2	0.17	0.70	3.1	<2.5	<2.5	<2.5	3.60
365	18.8	8.2	18.8	2.39	3.18	<0.2	0.28	1.12	<2.5	<2.5	<2.5	<2.5	3.26

Table 8
Ultrafiltered concentrations versus time during leaching of Pu-doped gel under reducing conditions

Time (Day)	Si (mg L^{-1})	B (mg L^{-1})	Na (mg L^{-1})	Li (mg L^{-1})	Ca (mg L^{-1})	Sr (mg L^{-1})	Al (mg L^{-1})	Fe (mg L^{-1})	Zr (μg L^{-1})	La (μg L^{-1})	Ce (μg L^{-1})	Nd (μg L^{-1})	Cs (mg L^{-1})
1	25.4	29.2	26.1	5.90	0.53	<0.2	0.17	1.20	16.0	<2.5	<2.5	<2.5	<0.2
7	32.0	22.2	29.8	4.14	0.77	<0.2	0.18	0.60	6.4	<2.5	<2.5	<2.5	<0.2
28	29.9	19.6	26.4	3.78	0.91	<0.2	0.26	0.52	4.5	<2.5	<2.5	<2.5	<0.2
90	34.8	21.2	28.6	4.14	1.66	<0.2	0.28	2.46	3.7	<2.5	<2.5	<2.5	<0.2
182	38.5	22.2	37.0	4.48	1.88	<0.2	0.23	0.68	2.5	<2.5	<2.5	<2.5	<0.2
365	53.2	22.4	73.3	4.68	6.48	<0.2	0.60	1.78	2.5	<2.5	<2.5	<2.5	<0.2

than 10 times lower than those measured. The ultrafiltered concentrations of the three rare earth elements and zirconium were distinctly lower than those of the other elements, i.e. about 10 ppb.

5. Gel alteration rates

The gel alteration rates are represented by the slope of the $NL(i) = f(t)$ lines, where i corresponds to a chemical element of the gel. Considering the gel leaching procedure, the normalized mass losses were calculated as follows:

$$NL(i)_{n=1} = \frac{1}{\tau_i \cdot SA} \cdot V_0 \cdot [i]_1,$$

$$NL(i)_{n\geqslant 2} = \frac{1}{\tau_i \cdot SA} \cdot \left[\left(V_0 - \sum_{j=1}^{j=n-1} V_j \right) \cdot [i]_j + \sum_{j=1}^{j=n-1} V_j \cdot [i]_j \right],$$

where V_0: leachate volume in the reactor at $t = 0$ (m^3); V_j: volume of the jth analysis sample (m^3); $[i]_j$: concentration of element i in the reactor during the jth sample (g m^{-3}); τ_i: mass concentration of element i in the gel (g_i/g_{gel}); SA: gel surface area in contact with the leachate (m^2).

The normalized mass losses were calculated on the assumption that the initial gel surface area did not vary during leaching. In fact, gel leaching probably results in a slight increase in the pore size rather than a decrease in the mean gel grain diameter and caused the specific surface area to increase with the percentage of altered gel. Conversely, assuming the gel alteration results in a decrease of gel grain diameter and silicon is a satisfactory gel alteration tracer, the shrinking core model yields a surface area decrease of about −10% after 1 year. Given this relatively low value and the fact that the two previous phenomena lead to opposite effects, the variation in the gel surface area during leaching was not taken into account in calculating the normalized mass losses. Conversely, the SA/V variation due to solution sampling for analysis was taken into account to calculate the NL values.

$NL(i)$ increased very significantly between 0 and 1 day, then, neglecting the data of 180 days, followed a generally linear variation between 7 days and 1 year (Fig. 6). The gel leaching behavior was clearly incongruent from the outset, with NL_{1d} values for the low-solubility elements (Al, Fe, Zr, REE) lower than the values for Si, Na, Li, Cs and Ca. Moreover, NL_{1d}(Si) was between 40% and 50% of the 1-year NL(Si) values. The same phenomenon was observed for the other soluble elements such as Na, Li, Cs and Ca, but with lower percentage values. By analogy with SON68 glass alteration, the initial time intervals (between 0 and 7 days) corresponded to dissolution of the gel at the initial rate, r_0,

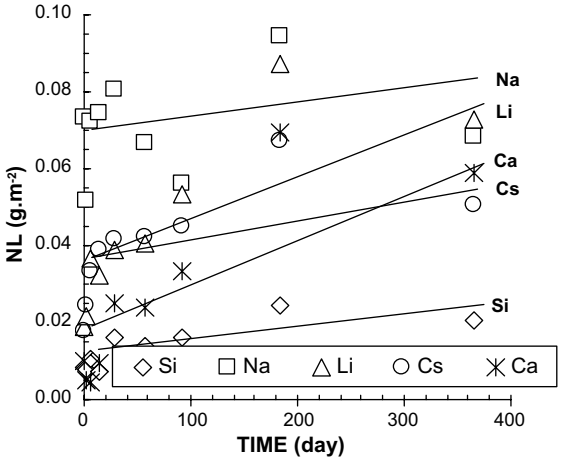

Fig. 6. Normalized mass losses versus time for silicon, sodium, lithium, cesium and calcium during leaching of Np-doped gel under oxidizing conditions.

followed by an extremely rapid rate drop; after 7 days the gel was altered under residual rate conditions. The high NL_{1d} values could also be attributed to preferential dissolution of the crystallized inclusions in the gel or to the dissolution of elements trapped in the gels pores during drying. The quantity of elements trapped in the gels during their drying can be estimate according to the following equation:

$$Q_g(i) = \omega \times \frac{M_g}{\rho_g} \times [i],$$

where $Q_g(i)$: mass of element i trapped inside the gel pores (g); ω: gel porosity; M_g: mass of gel (kg); ρ_g: gel density (2200 kg m^{-3}); $[i]$: concentration of element i in the leachate after complete alteration of glass monoliths (g m^{-3}).

Assuming a gel porosity of 0.5 (overestimated value) and considering the element concentrations measured during complete alteration of Am-doped glass (194, 2679, 2649, 230 and 10.4 mg L^{-1} respectively for Si, B, Na, Li and Ca), the mass of elements trapped inside the gel pores for 1 g of gel is 0.045, 0.616, 0.610, 0.053 and 0.002 mg for Si, B, Na, Li and Ca. The quantity of elements trapped in the Am-doped gel (for example) would represent only 0.3% of NL_{1d} for silicon and calcium, 5% for sodium and lithium, and 10% for boron. This hypothesis thus cannot account for the high NL_{1d} values. If the gels are assumed to be altered at the maximum rate, r_0, between 0 and 1 day, NL_{1d} would correspond to mean values of 0.013, 0.059 and 0.047 g m^{-2} d^{-1} when r_0 is calculated for silicon, sodium and lithium, respectively. These values are of the same order of magnitude as the initial rate (r_0) of SON68 glass at 50 °C and about pH 8 (0.025 g m^{-2} d^{-1}).

The gel alteration rates were calculated between 7 days and 1 year (Table 9). The $r(i)$ values calculated for americium-doped gel were generally higher than for the other gels, and the leachate redox potential, Eh, had no effect on $r(i)$ for neptunium- and plutonium-doped gels. The higher rates obtained with americium-doped gel may be due to the effect of direct radiolysis of the gel structure (depolymerization of the silicate network), or to an effect of the pH or SA/V ratio. Assuming the pH effect was the same for the gels as for the SON68 glass, the Am-doped gel alteration rates should have been only the half or the same of those of other gels, according to the gels dissolved in initial (r_0) [8] or residual [9] rate conditions. The pH hypothesis was therefore discounted. As the SA/V was not measured for the α-doped gels, the difference in the rate could be attributable to a different SA/V ratio for Am-doped gel. In this case, the same factor should be observed between the rates of the Am-doped gel and the mean rates, but it is contradicted by the different rate values. However, taking into account the uncertainty of gel alteration rates, the SA/V hypothesis cannot completely excluded. It is thus impossible to accurately determine whether the Am-doped gel alteration rates are due to γ radiolysis of the silicate network in the gel or to a different SA/V ratio.

Comparing the mean gel alteration rates yields the following relation: $Al \ll Si \approx Cs < Na \approx Ca < Li$. The three alkali metals thus do not exhibit the same leaching behavior, perhaps as a result of the presence of crystallized phases in the gels.

Table 9
Gel alteration rates calculated with respect to different elements between 7 days and 1 year

Gel	Rate (g m^{-2} d^{-1})						
	Si	Na	Li	Cs	Ca	Sr	Al
Non-rad.	$2.8 \pm 0.6 \times 10^{-5}$	$3.4 \pm 0.4 \times 10^{-5}$	$1.7 \pm 0.1 \times 10^{-4}$	–	$1.2 \pm 0.1 \times 10^{-4}$	$3.8 \pm 0.8 \times 10^{-5}$	–
Np ox	$3.8 \pm 0.9 \times 10^{-5}$	$2.1 \pm 3.4 \times 10^{-5}$	$1.2 \pm 0.3 \times 10^{-4}$	$5.4 \pm 2.7 \times 10^{-5}$	$1.7 \pm 0.2 \times 10^{-4}$	–	$3.7 \pm 1.2 \times 10^{-6}$
Pu ox	$2.9 \pm 0.8 \times 10^{-5}$	–	$1.3 \pm 0.4 \times 10^{-4}$	$4.4 \pm 0.7 \times 10^{-6}$	$2.3 \pm 0.3 \times 10^{-5}$	–	–
Am ox	$9.2 \pm 1.6 \times 10^{-5}$	$1.9 \pm 0.4 \times 10^{-4}$	$5.2 \pm 0.3 \times 10^{-4}$	$5.4 \pm 0.6 \times 10^{-5}$	$2.3 \pm 0.3 \times 10^{-4}$	$1.1 \pm 0.1 \times 10^{-4}$	–
Np red	$2.3 \pm 0.8 \times 10^{-5}$	$5.6 \pm 2.0 \times 10^{-5}$	$1.0 \pm 0.3 \times 10^{-4}$	$5.1 \pm 2.3 \times 10^{-5}$	$5.4 \pm 1.8 \times 10^{-5}$	–	$3.6 \pm 0.8 \times 10^{-6}$
Pu red	$5.4 \pm 0.7 \times 10^{-5}$	$1.8 \pm 0.7 \times 10^{-4}$	$4.7 \pm 1.5 \times 10^{-5}$	–	$8.8 \pm 1.2 \times 10^{-5}$	–	$8.1 \pm 1.9 \times 10^{-6}$
Average	$4.4 \pm 0.9 \times 10^{-5}$	$9.6 \pm 5.1 \times 10^{-5}$	$1.8 \pm 0.5 \times 10^{-4}$	$4.1 \pm 2.4 \times 10^{-5}$	$1.1 \pm 0.2 \times 10^{-4}$	$7.4 \pm 2.0 \times 10^{-5}$	$5.1 \pm 1.4 \times 10^{-6}$

The main alteration tracers in glass are boron, sodium and lithium. For the gels, however, only silicon can be considered as an alteration tracer because B, Na and Li are found in crystallized secondary phases. The quantity of secondary phases in the gels could not be measured, making it impossible to calculate the alteration rate for dissolution of the gel silicate network alone. Nevertheless, the low amplitude of the diffraction peaks (Fig. 2) for the secondary phases formed during gel fabrication at 300 °C indicates that the secondary phases were either present in small quantities or poorly crystallized. As the NL(i) values vary with $(SA/V)^{-1}$, the gel alteration rates $r(i)$ should vary with $(SA/V)^{-1}$ for elements such as Si and Al if the dissolution of the gel-forming network is controlled by a surface reaction. The dissolution rates of inactive gels formed at 90 °C were used for plotting the curves $r(i)$ versus the SA/V ratio. The gel dissolution rates obtained at three different SA/V ratios are plotted in Fig. 7, showing that they vary with $(SA/V)^n$. The r(Si) and r(Al) values are strongly dependent on the SA/V ratio (the exponent n is equal to -1.10 and -0.95, respectively, i.e. very near -1.0), whereas in the case of r(Na), n is equal to -0.14: the dissolution rates for the gel-forming elements Si and Al thus vary with $(SA/V)^{-1}$ whereas the Na dissolution rate is practically independent of the SA/V ratio. This indicates, taking into account the SA/V difference, that the dissolution rates are the same for the gels formed at 300° and 90 °C. Thus, the crystallized phases in the gels obtained at 300 °C do not modify the gel dissolution rate, either because they are found in negligible quantities, or because they dissolve at the same rate as the gel-forming network or with a lower rate. For calcium, the value of the exponent n is -1.07, very near those for silicon and aluminum. Calcium, which has a charge-compensating role in the gels, exhibits the same behavior as the gel network-forming elements, but with a higher dissolution rate (probably because of its higher solubility). These results indicate that the crystallized phases dissolution rate can be neglected with regards to that amorphous gel. They are consistent with a study [10] that showed that the dissolution rate was one order of magnitude lower for quartz than for SiO_2 glasses. The evolution of r(Na) versus the SA/V ratio indicates that sodium, and more generally the alkali metals, are preferentially included in the crystallized phases or phyllosilicates. These findings show that the amorphous gel dissolution rate can be considered equal to $4.4\times10^{-5}\,g\,m^{-2}\,d^{-1}$ at $44\,cm^{-1}$ and the crystallized phases dissolution neglected (for gel network forming elements: Si, Al).

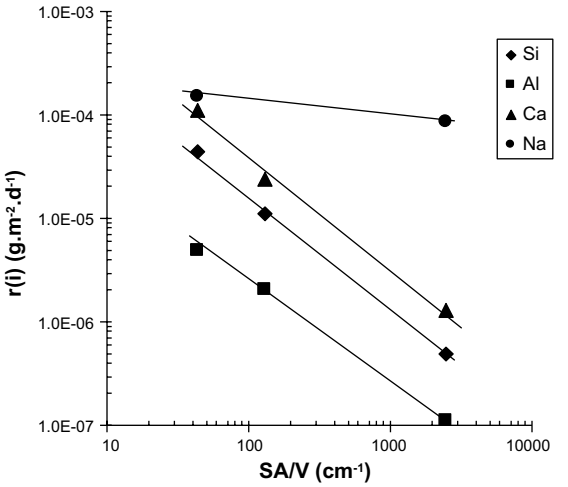

Fig. 7. Gel dissolution rates versus time at 50 °C calculated with respect to Si, Ca, Na and Al according to the SA/V ratio.

6. Behavior of the rare earth elements during gel leaching

The normalized mass losses were the same for the three rare earth elements (La, Ce, Nd), and were generally constant over time. The NL values for the rare earth elements are about 100 times lower than for silicon, corresponding to the solubilization of only about 1% of the REE during gel leaching. Considering cerium, under oxidizing conditions the major species in the leaching solution was Ce^{4+}, whereas under reducing conditions Ce^{3+} is supposed to predominate [11]. No difference between NL(La), NL(Ce) and NL(Nd) were observed and the NL(Ce) values were identical for the six leaching experiments, indicating that cerium behavior during gels leaching was not controlled by the oxidation–reduction potential of the solution.

The calculated solubility values of simple neodymium compounds were compared with the Nd concentrations measured in the leachate. As the three rare earth elements have exactly the same behavior, the calculations for Nd can be transposed to La and Ce. The dissociation constants (β) and solubility products (K) values were calculated at 50 °C using Helgeson's equation [12] for aqueous complexes and Van't Hoff's law for solid compounds. The expression for Helgeson's equation is given below:

$$\log\beta(T) = \frac{\Delta_r S^0_m(T_0)}{\ln 10\times RT} \times\left[T_0-\frac{\theta}{\omega}\left(1-\exp\left(\exp(b+aT)-c+\frac{T-T_0}{\theta}\right)\right)\right] -\frac{\Delta_r H^0_m(T_0)}{\ln 10\times RT},$$

with $a=0.01875\ K^{-1}$, $b=-12.741$, $c=7.84\times10^{-4}$, $\theta=219\ K$, $\omega=1.00322$, T_0: reference temperature

(298.15 K), $\Delta_r H^0_m$, $\Delta_r S^0_m$: standard molar enthalpy of reaction and standard molar entropy of reaction.

The Van't Hoff's law is given below:

$$\log K(T) = \log K(T_0) - \frac{\Delta_r H^0_m}{\ln 10 \times R} \times \left(\frac{1}{T} - \frac{1}{T_0}\right).$$

Sometimes, the thermodynamic data were not available to calculate β or K at 50 °C and consequently, the values at 25 °C were used by default (the values taken at 25 °C are indicated by an asterisk). Given the leachate composition, neodymium speciation and complexation calculations were based exclusively on aqueous hydroxides (OH^-), carbonates (HCO_3^- and CO_3^{2-}) and phosphates (HPO_4^{2-}). The following complexation reactions were taken into account:

$Nd^{3+} + H_2O \leftrightarrows NdOH^{2+} + H^+$	$\beta_1 = 10^{-7.63}$	[13]
$Nd^{3+} + 2H_2O \leftrightarrows Nd(OH)_2^+ + 2H^+$	$\beta_2 = 10^{-15.85}$	[13]
$Nd^{3+} + 3H_2O \leftrightarrows Nd(OH)_3 + 3H^+$	$\beta_3 = 10^{-24.51}$	[13]
$Nd^{3+} + 4H_2O \leftrightarrows Nd(OH)_4^- + 4H^+$	$\beta_4 = 10^{-34.43}$	[14]
$Nd^{3+} + CO_3^{2-} \leftrightarrows NdCO_3^+$	$\beta_1 = 10^{7.74}$	[15]
$Nd^{3+} + 2CO_3^{2-} \leftrightarrows Nd(CO_3)_2^-$	$\beta_2 = 10^{13.46}$	[15]
$Nd^{3+} + CO_3^{2-} + H^+ \leftrightarrows NdHCO_3^{2+}$	$\beta_1 = 10^{11.82}$	[15]
$Nd^{3+} + HPO_4^{2-} \leftrightarrows NdHPO_4^+$	$\beta_1 = 10^{4.29}$	[5]
$Nd^{3+} + 2HPO_4^{2-} \leftrightarrows Nd(HPO_4)_2^-$	$\beta_2 = 10^{7.08}$	[5]
$Nd^{3+} + HPO_4^{2-} + H^+ \leftrightarrows NdH_2PO_4^{2+}$	$\beta_1 = 10^{8.20}$	[5]

The total Nd concentration in solution was computed from the measured pH and calculated CO_2 fugacity at each sampling interval (see Section 4.1). Only the 1-year sample was used to calculate the $NdPO_4$ solubility. Because of the leachate pH, we considered that phosphorus was present in solution only as HPO_4^{2-} and that its concentration was proportional to the boron concentration ($[HPO_4^{2-}] \sim 10^{-5}$ mol L^{-1}). The following solid neodymium compounds and solubility products were considered:

$Nd(OH)_3(s) + 3H^+ \leftrightarrows Nd^{3+} + 3H_2O$	$K_s = 10^{17.0}$	[15]
$Nd_2(CO_3)_3(s) \leftrightarrows 2Nd^{3+} + 3CO_3^{2-}$	$K_s = 10^{-33.0}$*	[15]
$NdOHCO_3(s) \leftrightarrows Nd^{3+} + OH^- + CO_3^{2-}$	$K_s = 10^{-19.94\pm0.16}$*	[16]
$NdPO_4(s) + H^+ \leftrightarrows Nd^{3+} + HPO_4^{2-}$	$K_s = 10^{-12.80}$	[5]

The experimental and calculated neodymium solubilities for each sampling interval during leaching of Np-doped gel under oxidizing conditions are shown in Fig. 8. The same results were obtained for leaching of Pu- and Am-doped gels under oxidizing conditions. Neodymium phosphate $NdPO_4$ would result in Nd concentrations in solution about 1000 times lower than the measured values. This is not surprising insofar as the gels contain only 1 atom of phosphorus for 4 REE atoms (La + Ce + Pr + Nd); this compound therefore cannot control the neodymium solubility. Calculations also indicated that the neodymium solubility was not

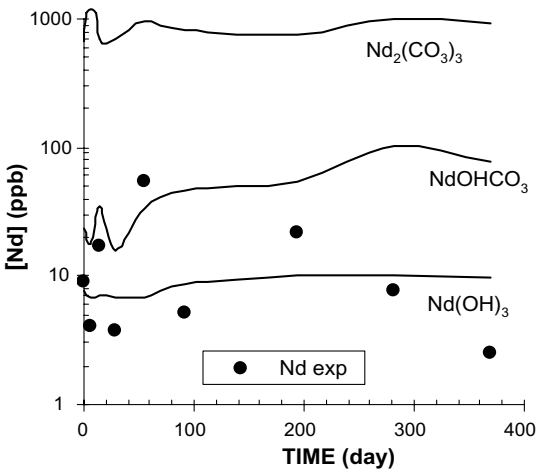

Fig. 8. Experimental and calculated neodymium solubility for three solid compounds during leaching of Np-doped gel under oxidizing conditions.

controlled by the carbonate $Nd_2(CO_3)_3$ because the total calculated Nd concentrations were about 2 orders of magnitude higher than the measured concentrations. Between 1 and 369 days, the neodymium solubility could be controlled by $Nd(OH)_3$ because the difference between the experimental and calculated concentrations was not very large (about 50%). Nevertheless, $NdOHCO_3$ cannot be completely excluded, at least for short durations, even if its solubility is greater than that of $Nd(OH)_3$ (a factor 3) because of the dispersion of the measured concentrations. For the last three sampling intervals, however, there was a substantial difference (about a factor 2–4) between the experimental and calculated solubility values. These results are partially consistent with the findings of an earlier leaching study with borosilicate glass [17], which showed that the neodymium solubility was controlled by $NdOHCO_3$ in the presence of carbon dioxide (CO_2 fugacity of 0.002 atm) and by $Nd(OH)_3$ without CO_2. According to the CO_2 fugacity evolution versus time during the gel leaching (Fig. 5), a fugacity of $10^{-3.5}$ atm is reached only for the last durations and this CO_2 fugacity is 10 times lower than that used for the glass leaching experiments in Ref. [17]. That could explain why in our experiments, the neodymium solubility would seem controlled by $Nd(OH)_3$ rather than $NdOHCO_3$. A TRLFS (time-resolved laser fluorescence spectroscopy) study of SON68 gels formed at 90 °C [18] showed that europium occupied two distinct sites in these materials. Nd^{3+} can be expected to exhibit the same leaching behavior as Eu^{3+}; it is thus unlikely that the neodymium solubility is controlled exclusively by a simple compound – particularly since one of the europium sites identified by TRLFS in the gels was a silicate site.

7. Actinide behavior during gel leaching

The concentrations measured in the leachates – unfiltered (d), filtered (f) to 0.45 μm, and ultrafiltered (uf) to 10 000 Dalton, i.e. a cutoff threshold of about 3 nm – are indicated in Table 10 (oxidizing conditions) and Table 11 (reducing conditions). The unfiltered Np, Pu and Am concentrations decreased (about a factor 2) between day 1 and day 14, then subsequently remained constant, whereas the ultrafiltered concentrations were roughly constant throughout. The same phenomenon has already been observed with low-solubility elements, and the difference between the unfiltered and filtered concentrations confirms the presence of gel particles in suspension even in the initial leachate samples. Assuming the gel particules to spheres (it is not really true) and using the Stokes' law, the settling rate of particles in suspension in the reactors versus their diameter can be calculated according to the following equation:

$$r_s = \frac{g \cdot d^2}{18} \times \frac{\rho_g - \rho_w}{\eta_w},$$

with ρ_g: gel density (2200 kg m^{-3}); ρ_w: water density at 50 °C (998 kg m^{-3}); η_w: water viscosity at 50 °C (0.549×10^{-3} kg m^{-1} s^{-1}); d: gel particle diameter (m); g: acceleration of gravity (9.81 m s^{-2}).

As the height of solution in the leaching reactors was about 15 cm and considering a settling time of 14 days, we find a Stokes' rate r_s of 1.24×10^{-7} m s^{-1}. This rate corresponds to the settling of gel particules of 0.3 μm diameter. This value of 0.3 μm is close to the cut-off size of filtered solutions (0.45 μm) and it is consistent with the fact that the filtered concentrations are roughly constant between 1 and 14 days (except for Np under oxidizing conditions). So, the gel particules settling could explain the decrease of the unfiltered concentrations between 1 and 14 days. The actinide concentration variations over time cannot be used to calculate the gel dissolution rates. The unfiltered actinide concentrations obtained after extended gel leaching were of the same order of magnitude as those measured during leaching of α-doped SON68 glass at 0.5 cm^{-1} and 50 °C [19]. The unfiltered, filtered and ultrafiltered Np and Pu concentrations obtained for the gel were also of the same order of magnitude as those measured during flowing leach tests at 90 °C with α-doped SON68 glass [20]. With silicon as the gel alteration tracer, the actinide retention factor in the gel is defined as follows:

$$\mathrm{RF(An)} = 1 - \frac{\mathrm{NL(An)_d}}{\mathrm{NL(Si)_d}}.$$

Three percentages corresponding to different cut-off sizes were calculated from analyzed concentrations:

$$\%(> 450\ \mathrm{nm}) = \frac{[\mathrm{An}]_d - [\mathrm{An}]_f}{[\mathrm{An}]_d} \times 100,$$

$$\%(3\text{–}450\ \mathrm{nm}) = \frac{[\mathrm{An}]_f - [\mathrm{An}]_{uf}}{[\mathrm{An}]_d} \times 100,$$

$$\%(< 3\ \mathrm{nm}) = \frac{[\mathrm{An}]_{uf}}{[\mathrm{An}]_d} \times 100.$$

Table 11
Np and Pu concentrations (μg L^{-1}) versus time (day) during gel leaching under reducing conditions: unfiltered (d), filtered to 0.45 μm (f), and ultrafiltered (uf)

Time	[Np] d	[Np] f	[Np] uf	[Pu] d	[Pu] f	[Pu] uf
1	929	155	2.4	162	8.3	1.40
7	836	256	2.3	45.3	5.7	0.03
28	764	239	2.3	17.0	7.9	0.05
90	697	366	–	16.1	4.0	0.25
182	691	320	6.9	15.3	4.1	0.32
365	1010	212	12.5	22.5	4.2	0.26

7.1. Neptunium

For the oxidizing medium, beyond 180 days, the ultrafiltered concentrations ($\sim 3 \times 10^{-7}$ M, Table 12) were identical with the filtered (0.45 μm) values. The colloidal Np percentage (>450 nm) increased slowly between 1 day and 1 year (Fig. 9) while in the same time, the colloidal Np percentage (3–450 nm) decreased to a very low value

Table 10
Np, Pu and Am concentrations (μg L^{-1}) versus time (day) during gel leaching under oxidizing conditions: unfiltered (d), filtered to 0.45 μm (f) and ultrafiltered (uf)

Time	[Np] d	[Np] f	[Np] uf	[Pu] d	[Pu] f	[Pu] uf	[Am] d	[Am] f	[Am] uf
1	2066	575	5.9	311	48.2	0.33	423	29.7	0.24
7	1532	377	4.1	167	27.6	0.06	224	52.2	0.17
14	1411	182	14.3	113	26.4	0.10	181	56.8	0.57
28	1150	172	12.1	115	30.4	0.09	144	45.4	0.09
56	1211	180	50.8	543	23.6	0.16	135	38.5	0.21
92	938	117	22.2	100	25.5	0.91	125	37.9	0.04
194	1123	101	53.9	85.0	22.1	0.71	114	30.3	0.15
282	1098	65.2	82.5	83.2	24.6	0.16	112	35.1	0.24
369	1148	70.8	65.0	71.0	31.4	1.13	113	35.6	1.11

Table 12
Ultrafiltered Np, Pu and Am concentrations (mol L^{-1}) versus time (day)

Time	Oxidizing medium			Reducing medium	
	[Np]	[Pu]	[Am]	[Np]	[Pu]
1	2.5×10^{-8}	1.4×10^{-9}	1.0×10^{-9}	1.0×10^{-8}	5.9×10^{-9}
7	1.7×10^{-8}	2.5×10^{-10}	7.1×10^{-10}	9.7×10^{-9}	1.1×10^{-10}
14	6.0×10^{-8}	4.0×10^{-10}	2.4×10^{-9}	–	–
28	5.1×10^{-8}	3.7×10^{-10}	3.7×10^{-10}	9.7×10^{-9}	2.1×10^{-10}
56	2.1×10^{-7}	6.6×10^{-10}	8.6×10^{-10}	–	–
90	–	–	–	–	1.0×10^{-9}
92	9.4×10^{-8}	3.8×10^{-9}	1.5×10^{-10}	–	–
182	–	–	–	2.9×10^{-8}	1.3×10^{-9}
194	2.3×10^{-7}	3.0×10^{-9}	6.4×10^{-10}	–	–
282	3.5×10^{-7}	6.6×10^{-10}	9.8×10^{-10}	–	–
365	-	–		5.3×10^{-8}	1.1×10^{-9}
369	2.7×10^{-7}	4.7×10^{-9}	4.6×10^{-9}	–	–

(<1%). The increase in the soluble Np percentage (<3 nm) with time was not only due to the gel dissolution but mainly came from the decrease of the (3–450 nm) percentage for the durations greater or equal to 92 days.

For the reducing medium, the ultrafiltered concentrations ($\sim5\times10^{-8}$ M) were about 6 times lower than under oxidizing conditions. The soluble neptunium concentration is thus sensitive to the Eh value of the leaching solution. The three percentages (>450 nm), (3–450 nm) and (<3 nm) remained roughly constant over time. In both cases (oxidizing and reducing conditions), the colloidal Np percentage (>450 nm) represented at least 70% of the total neptunium in solution.

The Pourbaix diagram calculated at 50 °C with the CHESS code indicates that two oxidation states (IV and V) for neptunium can exist in the reducing leachates. Given the Eh value, the NpO_2^+ and Np^{4+} relative quantities in solutions can be calculated according to the following redox equilibrium:

$$NpO_2^+ + 4H^+ + e^- \leftrightarrows Np^{4+} + 2H_2O,$$

$$E = E^0_{V/IV} - \frac{RT\ln 10}{F}\times\log\left(\frac{(Np^{4+})}{(NpO_2^+)\cdot(H^+)^4}\right),$$

with

$$E^0_{V/IV} = 0.604\ \text{V} \quad \text{and} \quad \frac{RT\ln 10}{F} = 0.064\ \text{at}\ 50\ ^\circ\text{C}.$$

The above equation leads to the following relative concentrations after 1 year of leaching:

$$\text{Oxidizing medium: } [Np^{4+}] = 9.8\times10^{-4}\times[NpO_2^+],$$

$$\text{Reducing medium: } [Np^{4+}] = 1.7\times10^{3}\times[NpO_2^+].$$

These calculations show that Np(V) largely predominates under oxidizing leaching and Np(IV) under reducing leaching. The difference between the ultrafiltered Np concentrations under oxidizing and reducing conditions is probably due to the difference in neptunium oxidation state. As Np(IV) tends to polymerize and thus form colloids, it is likely that in a reducing medium a fraction of the Np(V) is reduced to Np(IV), hence the increased colloid percentage (3–450 nm).

Neptunium speciation and complexation were calculated in solution to determine whether its solubility could be controlled by a simple compound. The complexants considered for the neptunium solubility calculations were OH^- and CO_3^{2-}. Similarly for neodymium, we used the measured pH and calculated CO_2 fugacity values for each sampling interval. The complexation and dissociation constants for aqueous and solid Np(V) species at 50 °C (*: value at 25 °C) were the following:

$$NpO_2OH + H^+ \leftrightarrows NpO_2^+ + H_2O \quad \beta_1 = 10^{10.48\pm0.7} \quad [21]$$

$$NpO_2(OH)_2^- + 2\ H^+ \leftrightarrows NpO_2^+ + 2H_2O \quad \beta_2 = 10^{22.01\pm0.5} \quad [21]$$

$$NpO_2^+ + CO_3^{2-} \leftrightarrows NpO_2CO_3^- \quad \beta_1 = 10^{5.56\pm0.06} \quad [21]$$

$$NpO_2^+ + 2CO_3^{2-} \leftrightarrows NpO_2(CO_3)_2^{3-} \quad \beta_2 = 10^{7.30\pm0.10} \quad [21]$$

$$NpO_2^+ + 3CO_3^{2-} \leftrightarrows NpO_2(CO_3)_3^{5-} \quad \beta_3 = 10^{5.33\pm0.15} \quad [21]$$

$$NpO_2^+ + 2CO_3^{2-} + OH^- \leftrightarrows NpO_2(CO_3)_2OH^{4-} \quad \beta_1 = 10^{8.70\pm1.16}* \quad [21]$$

$$NpO_2HCO_3 \leftrightarrows NpO_2^+ + H^+ + CO_3^{2-} \quad \beta_1 = 10^{-9.74\pm0.12} \quad [21]$$

$$1/2\ Np_2O_5(s) + H^+ \leftrightarrows NpO_2^+ + 1/2H_2O \quad K_s = 10^{3.36\pm0.02} \quad [21]$$

$$NpO_2OH(s) + H^+ \leftrightarrows NpO_2^+ + H_2O \quad K_s = 10^{4.14\pm0.5}(aged) \quad [21]$$

$$NaNpO_2CO_3(s) \leftrightarrows Na^+ + NpO_2^+ + CO_3^{2-} \quad K_s = 10^{-11.66\pm0.5}* \quad [21]$$

$$Na_3NpO_2(CO_3)_2(s) \leftrightarrows 3Na^+ + NpO_2^+ + 2CO_3^{2-} \quad K_s = 10^{-14.22\pm0.66} \quad [22]$$

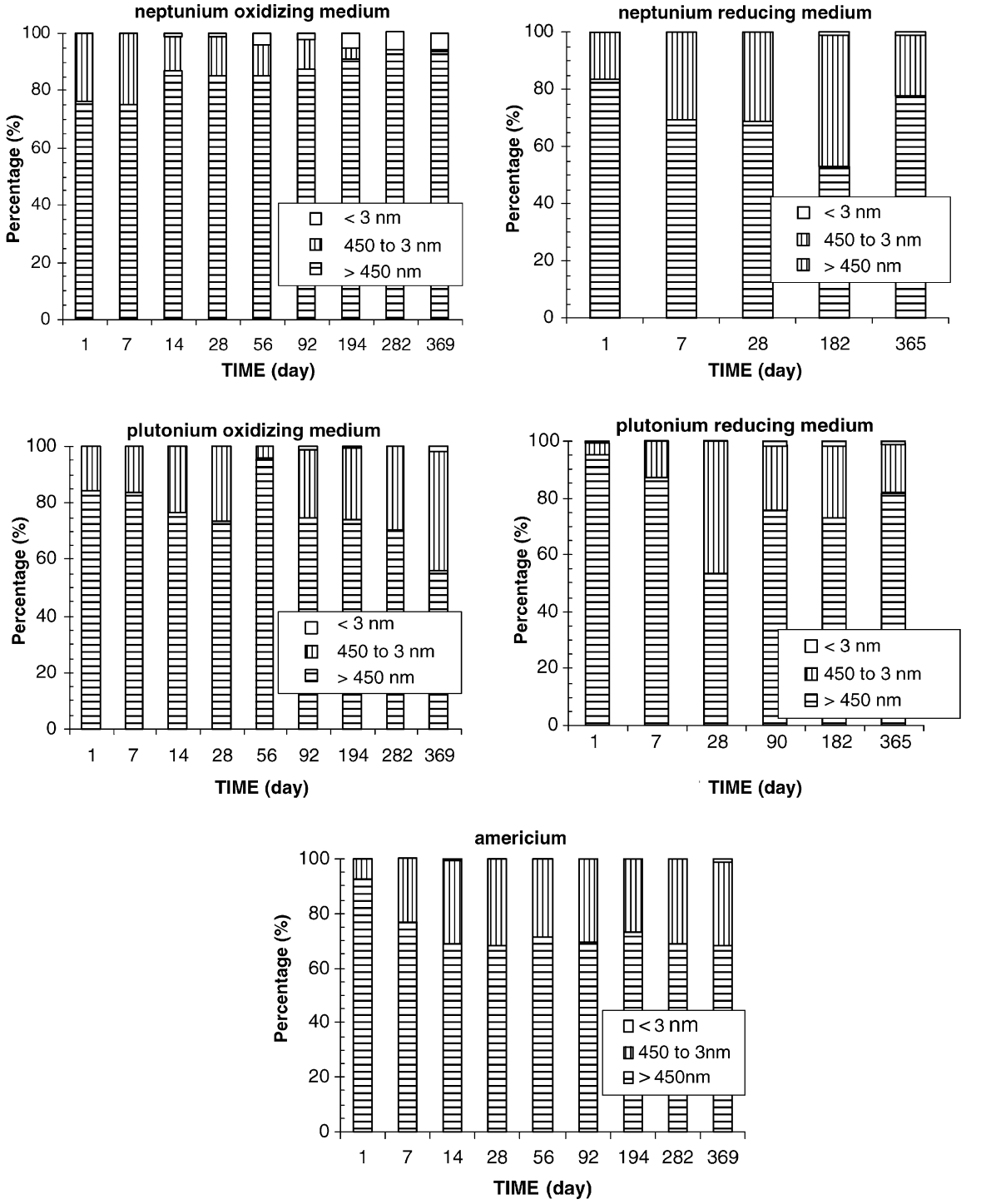

Fig. 9. Distribution of actinides among the particle fraction exceeding 450 nm, the particle fraction between 450 and 3 nm and the dissolved fraction smaller than 3 nm.

For Np(IV), the following reactions were taken into account for the solubility calculations:

$$Np^{4+} + H_2O \leftrightarrows NpOH^{3+} + H^+ \quad \beta_1 = 10^{-0.29\pm1.0} \quad [21]$$
$$Np^{4+} + 4H_2O \leftrightarrows Np(OH)_4 + 4H^+ \quad \beta_4 = 10^{-9.8\pm1.1} \quad [21]$$
$$Np^{4+} + 4CO_3^{2-} \leftrightarrows Np(CO_3)_4^{4-} + 4H^+ \quad \beta_4 = 10^{36.7}* \quad [21]$$
$$Np^{4+} + 5CO_3^{2-} \leftrightarrows Np(CO_3)_5^{6-} + 4H^+ \quad \beta_5 = 10^{35.6}* \quad [21]$$
$$Np(OH)_4(s) + 4H^+ \leftrightarrows Np^{4+} + 4H_2O \quad K_s = 10^{0.74} \quad [15]$$

None of the Np(V) compounds tested could account for the experimental neptunium solubility under either oxidizing or reducing conditions. The neptunyl sodium carbonates $NaNpO_2CO_3$ and $Na_3NpO_2(CO_3)_2$ are highly soluble: $\sim10^{-3}$ M and $\sim10^{4}$ M, respectively. Depending on the CO_2 fugacity and pH values, the calculated Np_2O_5 solubility ranges from 1.9×10^{-5} to 7.2×10^{-5} mol L^{-1} in oxidizing media and from 2.2×10^{-7} to 1.5×10^{-5} mol L^{-1} in reducing media. The NpO_2OH solubility ranges from 1.1×10^{-4} to 4.4×10^{-4} mol L^{-1} in oxidizing media and from 4.1×10^{-5} to 9.3×10^{-5} mol L^{-1} in reducing media, whereas the experimental concentrations after 6 months or more were about 3×10^{-7} and 5×10^{-8} mol L^{-1} in oxidizing and reducing media, respectively. The experimental Np concentrations were thus well below those calculated for the different compounds. The calculated solubility for $Np(OH)_4$ under reducing conditions was 7.4×10^{-11} mol L^{-1}, much lower than the Np concentrations measured in the leachate. No Np(V) or Np(IV) simple compound controls the neptunium solubility, neither under oxidizing medium nor reducing medium, even taking into account the uncertainties on β and K values.

The neptunium retention factor RF(Np) in the gels was about 0.35 for the oxidizing medium and about 0.50 for the reducing medium. Thus only 65% (oxidizing medium) or 50% (reducing medium) of the Np present in the gels was released into solution, and the soluble amount (<3 nm) represented no more than a few percent of the quantity potentially available for leaching.

7.2. Plutonium

For the oxidizing medium, the ultrafiltered concentrations ($\sim4\times10^{-9}$ M, Table 12) were well below the concentrations filtered to 0.45 μm (by a factor of 30). The colloidal Pu percentage (>450 nm) decreased from 1 day to 1 year while in the same time the colloidal Pu percentage (3–450 nm) increased (Fig. 9). The soluble Pu percentage (<3 nm) was small and constant, representing about 1% of the plutonium released from the gel. The plutonium behavior was in contrary to that of neptunium (this could mean different oxidation states for neptunium and plutonium).

For the reducing medium, the ultrafiltered concentrations ($\sim10^{-9}$ M) were about 4 times lower than under oxidizing conditions; the soluble plutonium concentrations are therefore sensitive to the Eh value of the leachate. The distribution of the different percentages (>450 nm), (3–450 nm) and (<3 nm) was roughly the same as that of neptunium. This could indicate that under reducing conditions, Np and Pu were at the same oxidation state.

The Pourbaix diagram calculated at 50 °C with the CHESS code indicates that two oxidation states for plutonium can exist in the oxidizing (V and IV) and reducing (IV and III) leachates. The PuO_2^+, Pu^{4+} and Pu^{3+} relative concentrations in solutions can be calculated versus the Eh value according to the two following redox equilibria:

$$PuO_2^+ + 4H^+ + e^- \leftrightarrows Pu^{4+} + 2H_2O \quad (1)$$

$$E = E^0_{V/IV} - \frac{RT\ln 10}{F} \times \log\left(\frac{(Pu^{4+})}{(PuO_2^+)\cdot(H^+)^4}\right)$$

with $E^0_{V/IV} = 1.031$ V

and

$$Pu^{4+} + e^- \leftrightarrows Pu^{3+} \quad (2)$$

$$E = E^0_{IV/III} - \frac{RT\ln 10}{F} \times \log\left(\frac{(Pu^{3+})}{(Pu^{4+})}\right) \quad \text{with } E^0_{IV/III} = 1.047\,\text{V}.$$

The above equations lead to the following relative concentrations after 1 year of leaching:

Oxidizing medium: $[Pu^{4+}] = 4.2\times10^7 \times [PuO_2^+]$, (1)

Reducing medium: $[Pu^{4+}] = 6.8\times10^4 \times [Pu^{3+}]$. (2)

These calculations show that plutonium is mainly at the oxidation state IV because Pu^{4+} is the prevalent species in solution, as well under oxidizing conditions as under reducing conditions. This could account for the fact that the soluble Pu percentage (<3 nm) is not sensitive to the Eh value within the range studied, Pu(IV) forming colloids much more readily than Pu(III) and Pu(V) [23].

Plutonium speciation and complexation were calculated in solution to determine whether its solubility could be controlled by a simple compound. The same complexants were considered as for the neodymium solubility calculations, i.e. OH^-, CO_3^{2-} and HPO_4^{2-}. Similarly, we used the measured pH values and calculated CO_2 fugacity values for each sampling interval. The HPO_4^{2-} concentrations were determined as described in Section 6. Although under reducing conditions plutonium is at the oxidation state IV, the solubility with regard to $Pu(OH)_3$ has been tested. The complexation and dissociation constants for aqueous and solid Pu(IV) species at 50 °C (*: value at 25 °C) were the following:

$$Pu^{4+} + H_2O \leftrightarrows PuOH^{3+} + H^+$$
$$\beta_1 = 10^{-0.26\pm0.60} \quad [21]$$
$$Pu^{4+} + 2H_2O \leftrightarrows Pu(OH)_2^{2+} + 2H^+$$
$$\beta_2 = 10^{-0.48} \quad [15]$$
$$Pu^{4+} + 3H_2O \leftrightarrows Pu(OH)_3^{+} + 3H^+$$
$$\beta_3 = 10^{-3.13} \quad [15]$$
$$Pu^{4+} + 4H_2O \leftrightarrows Pu(OH)_4 + 4H^+$$
$$\beta_4 = 10^{-7.20} \quad [15]$$
$$PuCO_3^{2+} \leftrightarrows Pu^{4+} + CO_3^{2-}$$
$$\beta_1 = 10^{-18.92} \quad [14]$$
$$Pu(CO_3)_2 \leftrightarrows Pu^{4+} + 2CO_3^{2-}$$
$$\beta_2 = 10^{-33.50} \quad [14]$$
$$Pu(CO_3)_3^{2-} \leftrightarrows Pu^{4+} + 3CO_3^{2-}$$
$$\beta_3 = 10^{-42.92} \quad [14]$$
$$Pu(CO_3)_4^{4-} \leftrightarrows Pu^{4+} + 4CO_3^{2-}$$
$$\beta_4 = 10^{-37.0}* \quad [22]$$
$$Pu(CO_3)_5^{6-} \leftrightarrows Pu^{4+} + 5CO_3^{2-}$$
$$\beta_5 = 10^{-35.6}* \quad [22]$$
$$PuHPO_4^{2+} \leftrightarrows Pu^{4+} + HPO_4^{2-}$$
$$\beta_1 = 10^{-14.46} \quad [5]$$
$$Pu(HPO_4)_2 \leftrightarrows Pu^{4+} + 2HPO_4^{2-}$$
$$\beta_2 = 10^{-25.06} \quad [5]$$
$$Pu(HPO_4)_3^{2-} \leftrightarrows Pu^{4+} + 3HPO_4^{2-}$$
$$\beta_3 = 10^{-34.33} \quad [5]$$
$$Pu(HPO_4)_4^{4-} \leftrightarrows Pu^{4+} + 4HPO_4^{2-}$$
$$\beta_4 = 10^{-42.30} \quad [5]$$
$$Pu(OH)_4(s) \leftrightarrows Pu^{4+} + 4OH^-$$
$$K_s = 10^{-55.96\pm1} \quad [21]$$

For Pu(III), the following reactions were taken into account for the solubility calculations:

$$Pu^{3+} + H_2O \leftrightarrows PuOH^{2+} + H^+ \quad \beta_1 = 10^{-6.18\pm0.3} \quad [21]$$
$$Pu^{3+} + CO_3^{2-} \leftrightarrows PuCO_3^{+} \quad \beta_1 = 10^{7.56} \quad [21]$$
$$Pu^{3+} + 2CO_3^{2-} \leftrightarrows Pu(CO_3)_2^{-} \quad \beta_2 = 10^{12.72} \quad [21]$$
$$Pu(OH)_3(s) + 3H^+ \leftrightarrows Pu^{3+} + 3H_2O \quad K_s = 10^{13.72\pm1.5} \quad [21]$$

For most durations under oxidizing conditions, the plutonium concentrations calculated from $Pu(OH)_4$ solubility (Fig. 10) were higher than those measured. The agreement between experimental and plutonium concentrations calculated from $Pu(OH)_3$ solubility was not really better than for $Pu(OH)_4$, except for 92 and 194 days. Under reducing conditions (Fig. 11), $Pu(OH)_3$ and $Pu(OH)_4$ solubilities were close and did not account for the experimental concentrations beyond 3 months. The similarity of the differences (by a factor about 5) between

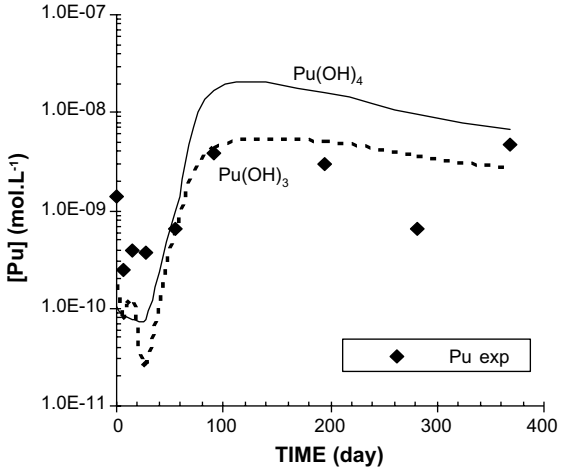

Fig. 10. Experimental and calculated plutonium solubility for $Pu(OH)_4$ and $Pu(OH)_3$ during gel leaching under oxidizing conditions.

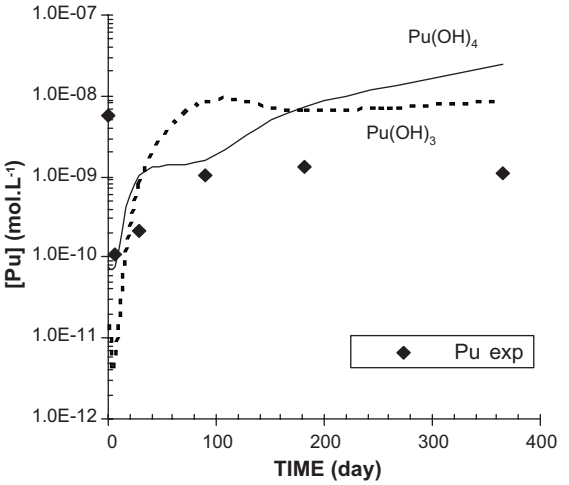

Fig. 11. Experimental and calculated plutonium solubility for $Pu(OH)_4$ and $Pu(OH)_3$ during gel leaching under reducing conditions.

the experimental concentrations and the $Pu(OH)_4$ solubility in oxidizing and reducing media is consistent with the calculated Pu(IV) state in the both media. Thus, neither $Pu(OH)_4$ nor $Pu(OH)_3$ seem to control the plutonium solubility, except if the incertitude on K is taken into account; in this case, the best agreement for the both leaching experiments would be obtained for $Pu(OH)_4$, that would be consistent with the presence of Pu(IV) in solutions.

The plutonium retention factor RF(Pu) in the gels was about 0.93 for the oxidizing medium and about 0.98 for the reducing medium. Thus only 7% (oxidizing medium) and 2% (reducing medium) of the Pu present in the gels was released into solution, and the soluble

concentrations (<3 nm) represented no more than a thousandth of the total plutonium in solution.

7.3. Americium

The ultrafiltered concentrations appeared to be constant throughout the alteration period at about 10^{-9} mol L^{-1} (Table 12), two orders of magnitude below the filtered concentrations. The three percentages (>450 nm), (3–450 nm) and (<3 nm) remained constant beyond 1 day of leaching, as indicated by Fig. 9. The distribution of the different percentages versus time was comparable to that obtained for plutonium leached under reducing conditions.The soluble Am percentage (<3 nm) represented only 0.1–1% of the total americium in solution.

Speciation and complexation calculations were carried out for americium in solution, as for neodymium, neptunium and plutonium. Only Am(III) was taken into account in this case. The same anionic complexants were considered as for the neodymium solubility calculations, i.e. OH^-, CO_3^{2-} and HPO_4^{2-}. Similarly, we used the measured pH values and calculated CO_2 fugacity values for each sampling interval. The HPO_4^{2-} concentration after 1 year was determined as described in Section 6. The complexation and dissociation constants for aqueous and solid Am(III) species at 50 °C (*: value at 25 °C) were the following:

$$Am^{3+} + H_2O \leftrightarrows AmOH^{2+} + H^+ \quad \beta_1 = 10^{-7.07\pm0.7} \quad [22]$$

$$Am^{3+} + 2H_2O \leftrightarrows Am(OH)_2^+ + 2H^+ \quad \beta_2 = 10^{-15.86\pm0.6} \quad [22]$$

$$Am^{3+} + 3H_2O \leftrightarrows Am(OH)_3 + 3H^+ \quad \beta_3 = 10^{-25.29\pm0.5} \quad [22]$$

$$Am^{3+} + CO_3^{2-} \leftrightarrows AmCO_3^+ \quad \beta_1 = 10^{8.00\pm0.3} \quad [24]$$

$$Am^{3+} + 2CO_3^{2-} \leftrightarrows Am(CO_3)_2^- \quad \beta_2 = 10^{13.03\pm0.4} \quad [24]$$

$$Am^{3+} + 3CO_3^{2-} \leftrightarrows Am(CO_3)_3^{3-} \quad \beta_3 = 10^{15.87\pm0.6} \quad [24]$$

$$Am^{3+} + H^+ + HPO_4^{2-} \leftrightarrows AmH_2PO_4^{2+} \quad \beta_1 = 10^{9.65\pm0.5} \quad [24]$$

$$Am(OH)_3(s)_{cr,am} + 3H^+ \leftrightarrows Am^{3+} + 3H_2O$$

$$K_{s,cr} = 10^{13.83\pm0.6} \quad [22]$$

$$K_{s,am} = 10^{15.13\pm0.6} \quad [22]$$

$$AmOHCO_3(s) \leftrightarrows Am^{3+} + CO_3^{2-} + OH^- \quad K_s = 10^{-18.02\pm1.4} \quad [22]$$

$$0.5\ Am_2(CO_3)_3(s) \leftrightarrows Am^{3+} + 1.5CO_3^{2-} \quad K_s = 10^{-13.24\pm1.1} \quad [24]$$

$$NaAm(CO_3)_2(s) \leftrightarrows Na^+ + Am^{3+} + 2CO_3^{2-} \quad K_s = 10^{-17.56}* \quad [24]$$

$$AmPO_4(s) + H^+ \leftrightarrows Am^{3+} + HPO_4^{2-} \quad K_s = 10^{-12.44\pm0.6}* \quad [24]$$

Sodium americium carbonate $NaAm(CO_3)_2$ yielded very high Am concentrations (about 10^{-1} mol L^{-1}) in solution. Americium phosphate $AmPO_4$, resulted in very low Am concentrations ($\sim 3\times10^{-13}$ mol L^{-1}). It is not surprising that this compound does not control the americium solubility, as there is not enough phosphorus in the gels to complex all the rare earth elements and americium. After 1 month or more, $Am_2(CO_3)_3$ and $AmOHCO_3$ yielded americium concentrations in the leachates of $\sim 4\times10^{-3}$ and $\sim 3\times10^{-5}$ mol L^{-1}, respectively. These calculated concentrations were too much higher than the concentrations measured in the leachates. The amorphous and crystallized $Am(OH)_3$ yielded Am concentrations higher than those measured, as shown on Fig. 12. The closest values from experimental concentrations were obtained for crystallized americium hydroxide but they were 1 order of magnitude higher than the experimental data, therefore the solubility of americium was not controlled by any simple phase. This is rather surprising, considering that the agreement between Nd experimental concentrations and $Nd(OH)_3$ solubility was not too bad and that neodymium is generally acknowledged to be a satisfactory americium surrogate and therefore these two elements should exhibit the same chemical behavior.

The americium retention factor RF(Am) in the gel was 0.94: only 6% of the americium in the gel was released into the leachate, and the soluble Am amount (<3 nm) represented less than one thousandth of the quantity of americium potentially available for leaching. The leach tests with α-doped gels showed that americium exhibits the same behavior as plutonium under reducing conditions.

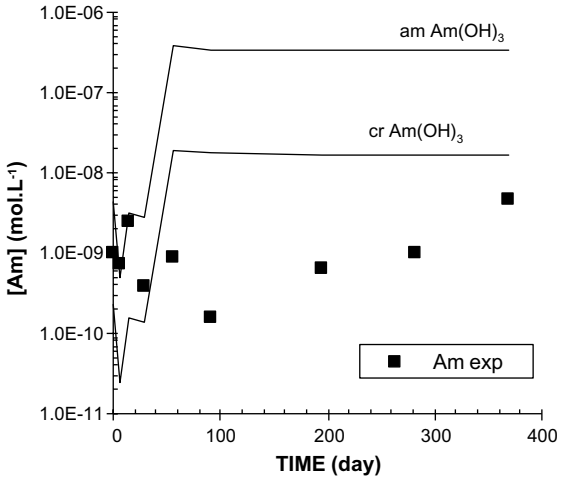

Fig. 12. Experimental and calculated americium solubility for amorphous and crystallized $Am(OH)_3$ during gel leaching.

7.4. Discussion

The simple solubility calculations described in the preceding section show that the actinide concentrations in solution are not controlled by pure phases. Given specific surface area of the gels, the possible presence of adsorbed actinides can be considered. In the case of the SON68 gel formed at 90 °C, it was shown [25] that the adsorption percentage of neptunium and americium on this material was very close to 100% beyond pH value of 9 and 6 respectively. This study showed that the actinide sorption reaction on the gel can be expressed as follows:

$$\mathrm{SOH} + \mathrm{An}^{m+} \leftrightarrows \mathrm{SOAn}^{(m-1)+} + \mathrm{H}^{+}$$

Assuming the An concentrations in solution arise from the dissolution of a pure phase in the gel, allowance for An adsorption on the gel will not modify the concentrations, which will continue to be governed by the dissolution of a pure gel phase. Adsorption would simply enhance the dissolution of the pure phase to reach the concentration at the equilibrium with the pure phase considered. Conversely, assuming the actinide is incorporated in the gel as an end-member in an ideal solid solution composed of the mean elements of the gel (taken under oxide or hydroxide form), the actinide concentration in solution would correspond to the solubility of the An end-member given by the ideal solid solution precipitation, corrected for adsorption. This kind of calculation would lead to An concentrations in solution lower than those calculated by only the ideal solid solution precipitation. The ideal solid solutions model applied to inactive simplified glasses with 4 and 6 elements allowed to correctly simulate the gels composition [26]. Coupling the ideal solid solutions model with the actinides adsorption should be an interesting way to simulate the An concentrations in solution during gel (or glass) leaching.

8. Conclusion

Gels formed by hydrothermal alteration of α-doped (Np, Pu, Am) SON68 glass at 300 °C were leached in static mode at 50 °C and 44 cm^{-1} under oxidizing conditions (Eh $\sim +150$ mV) and under reducing conditions (Eh ~ -250 mV). During glass alteration, several crystallized secondary phases formed together with the amorphous gel.

The gel dissolution was highly incongruent from the outset (day 1). The gel dissolution rate appears to correspond mainly to dissolution of the amorphous gel because the crystallized phases dissolution rate can be neglected for network forming elements (Si, Al). Using the silicon release as a gel alteration tracer, the mean gel dissolution rate was 4.4×10^{-5} $\mathrm{g\,m^{-2}\,d^{-1}}$ at an SA/V ratio of 44 cm^{-1}. The dissolution rate of the Am-doped gel was about twice higher than those of the other, but it is impossible to determine whether it was an effect of the pH (0.5 unit lower than for inactive, Np- and Pu-doped gel leaching) or of γ radiolysis due to americium on gel silicated network. Cesium entered solution at a lower rate than sodium and lithium, but comparable to silicon.

The three rare earth elements (La, Ce, Nd) exhibited exactly the same behavior during leaching, irrespective of the actinide with which the gels were doped. Speciation and complexation calculations showed that the neodymium solubility could be perhaps controlled by $Nd(OH)_3$, at least beyond 3 months of leaching.

The neptunium concentration in solution was sensitive to the redox potential of the leaching solution, at about 3×10^{-7} mol L^{-1} under oxidizing conditions and 5×10^{-8} mol L^{-1} under reducing conditions. Calculations based on the redox equilibria showed that the main oxidation state of neptunium was the oxidation state V under oxidizing conditions, and the oxidation state IV under reducing conditions, which led to a higher Np colloidal amount in this medium. Neptunium is weakly retained in the gel during leaching: about 65% of the leachable Np is released into solution in oxidizing media and 50% in reducing media. However, the soluble Np concentrations (<3 nm) in the leachate represent only a few percent of the total Np in solution. Plutonium is slightly less sensitive to the redox potential of the solution: concentrations of 4×10^{-9} and 10^{-9} mol L^{-1} were measured in oxidizing and reducing media, respectively. Calculations based on the redox equilibria led to oxidation state IV for plutonium under oxidizing and reducing conditions. The americium concentration in the leachate was about 10^{-9} mol L^{-1}. Plutonium and americium were strongly retained in the gel regardless of the redox conditions, and less than 10% of the Pu and Am were released into the leachates. Moreover, the soluble Pu and Am concentrations (<3 nm) in the leachates represented less than a thousandth of the total Pu and Am in solution. Solubility calculations showed that actinides concentrations in solution were not controlled by the precipitation of simple phases (hydroxide or carbonate). These experiments also showed that not only the actinides but also the other elements having a low solubility (Al, Fe, ...) had a complicated behavior during gels leaching. To simulate the actinides concentrations in solution, the ideal solid solutions model coupled with the actinides adsorption on the gel pores surface should be an interesting way to explore.

The gel leaching behavior showed that the actinides trapped in the gel during glass alteration are very strongly confined with very low solubility, even in an accident situation where glass is in contact with groundwater at high temperature. These leaching experiments showed that the neptunium and plutonium release from

the gels would be decreased by the reducing conditions expected in a repository site.

Acknowledgments

The authors thank Dr. Mireilla Del Nero for fruitful discussions. The authors are grateful to Dr. J.L. Dautheribes, A. Gavazzi, and C. Marques for ICP-MS, ICP-AES and α spectrometry analyses and to the European Community for funding of this study under the 5th PCRD 1999-2003 (GLASTAB project, contract FIKW-CT-2000-00007).

References

[1] Y. Etoh, H. Karasawa, E. Ibe, M. Sakagami, J. Nucl. Sci. Technol. 24 (1987) 672.
[2] H. Karasawa, E. Ibe, S. Uchida, Y. Etoh, T. Yasuda, Radiat. Phys. Chem. 37 (1991) 193.
[3] Z. Cai et al., Nucl. Technol. 136 (2) (2001) 231.
[4] F. Delage, D. Ghaleb, J.L. Dussossoy, O. Chevalier, E. Vernaz, J. Nucl. Mater. 190 (1992) 191.
[5] T. Wolery, UCLA-MA-110662 PTI ed., LLNL, 1992.
[6] T. Advocat, PhD thesis, University of Strasbourg, 1991.
[7] J. Van der Lee, Technical Report LHM/RD/98-39, CIG, School of Mines of Paris, France, 1998.
[8] T. Advocat, J.L. Crovisier, E. Vernaz, G. Ehret, H. Charpentier, Mater. Res. Soc. Symp. Proc. 212 (1990) 57.
[9] S. Gin, J.P. Mestre, J. Nucl. Mater. 295 (2001) 83.
[10] J.P. Icenhower, P.M. Dove, Geochim. Cosmochim. Acta 64-24 (2000) 4193.
[11] S.A. Hayes, P. Yu, T.J. O'Keefe, M.J. O'Keefe, J.O. Stoffer, J. Electrochem. Soc. 149 (2002) 623.
[12] H.C. Helgeson, J. Phys. Chem. 71 (1967) 3121.
[13] J.H. Lee, R.H. Byrne, Geochim. Cosmochim. Acta 56 (1992) 1127.
[14] D.G. Brookins, in: Lipin, McKay (Eds.), Review in Mineralogy, vol. 21, The Mineralogical Society of America, Washington, 1989, p. 201.
[15] W.E. Falck, D. Read, J.B. Thomas, Chemval 2: thermodynamic data base, EUR 16897 EN, 1996.
[16] W. Runde, G. Meinrath, J.I. Kim, Radiochim. Acta 58&59 (1992) 93.
[17] D. Rai, A.R. Felmy, R.W. Fulton, J.L. Ryan, Radiochim. Acta 58&59 (1992) 9.
[18] N. Ollier et al., J. Lumin. 94&95 (2001) 197.
[19] S. Fillet, PhD thesis, University of Montpellier, 1987.
[20] O. Menard, T. Advocat, J.P. Ambrosi, A. Michard, Appl. Geochem. 13 (1998) 105.
[21] R.J. Lemire et al., Chemical Thermodynamics of Neptunium and Plutonium, vol. 4, 2001.
[22] R. Guillaumont, Update on the Chemical Thermodynamics of U, Np, Pu, Am and Tc, vol. 5, 2003.
[23] J. Kim, Radiochim. Acta 52&53 (1991) 71.
[24] R.J. Silva, Chemical Thermodynamics of Americium, vol. 2, 1995.
[25] I. Ribet et al., Glastab EC project, contract FIKW-CT-2000-00007, final report, 2004.
[26] I. Munier et al., J. Nucl. Mater. 324 (2004) 97.